QUIET DRONES 2026
Delft, 29th June - 1st July 2026

On the psychoacoustic impact of synchrophasing for distributed propellers and ducted fans

Session: Auralization and Acoustic Simulation

Stephen Schade, German Aerospace Center, Bismarckstraße 101, 10625 Berlin, Germany, stephen.schade@dlr.de
Maximilian Marggraf, German Aerospace Center, Bismarckstraße 101, 10625 Berlin, Germany, maximilian.marggraf@dlr.de
Roberto Merino-Martinez, Delft University of Technology, Faculty of Aerospace Engineering, 2629 HS Delft, the Netherlands, R.MerinoMartinez@tudelft.nl
Karl-Stéphane Rossignol, German Aerospace Center, Lilienthalplatz 7, 38108 Braunschweig, Germany, Karl-Stephane.Rossignol@dlr.de
Sébastien Guérin, German Aerospace Center, Bismarckstraße 101, 10625 Berlin, Germany, sebastien.guerin@dlr.de

Abstract This study examines whether synchrophasing and stator clocking can reduce tonal noise emissions in distributed propulsion systems under realistic flight conditions. Using measurement-informed auralization, we evaluate two configurations: an eight-propeller tilt-prop aircraft and a tilt-duct system with 26 fans. For the distributed propellers, results demonstrate that synchrophasing at specific phase angles (e.g. half propeller blade-to-blade angle) induces destructive interference at the blade-passing frequency and its harmonics, leading to sound pressure level reductions of approximately 10 dB and a reduction of tonality and fluctuation strength larger than one just-noticeable difference compared to in-phase operation. For the ducted fans, an evolutionary optimization routine determines optimal stator clocking positions to minimize tonal interaction noise. This approach achieves tonal noise reduction of approximately 10 dBA at centerline certification positions. Whereas the optimized stator distribution successfully lowers centerline noise levels by creating a narrow low-tonal noise corridor beneath the flight path, a significant lateral reduction (e.g. for surrounding communities) could not be achieved. The findings establish phase control and stator clocking as viable, yet sensitive, degrees of freedom for minimizing tonal noise in distributed propulsion systems.

Keywords: Psychoacoustics; Synchrophasing; Distributed Propulsion; Urban Air Mobility

1. Introduction

Synchrophasing has emerged as a potential strategy to mitigate tonal noise for distributed, electric propeller arrays by specifically adjusting the relative blade-phase angle $\Delta\phi$ between adjacent propellers. Lafuente et al. (Lafuente, Pulzovan, Cepeda-Gomez, & Geyer, 2025) conduct a parametric investigation showing that extremum-seeking control with Extended Kalman Filter gradient estimation can yield noise reductions of up to $15\,\mathrm{dB}$ across various propeller layouts. Experimental work by Monteiro et al. (d. Monteiro, Merino-Martinez, & Pereira, 2024) indicates that specific relative blade-phase angles can significantly reduce loudness, tonality, and overall psychoacoustic annoyance in wind-tunnel conditions for simple propeller arrays. The authors conclude that tonal noise radiation can be reduced when $\Delta\phi$ approximates half the propeller blade-to-blade angle (e.g. $\Delta\phi = 30\,\mathrm{deg}$ for a six-bladed propeller). Numerical simulations by Zarri et al. (Zarri, Koutsoukos, & Avallone, 2023) reveal that synchrophasing of three co-rotating propellers reduces tonal noise through destructive interference while leaving aerodynamic performance mainly unaffected. Guérin and Tormen (Guérin & Tormen, 2023) further highlight the sensitivity of acoustic directivity to initial relative blade positions in multi-propeller configurations, raising questions about how these effects transfer to more realistic aircraft geometries. Patterson et al. (Patterson, Ackerman, Hovakimyan, & Gregory, 2021) extend the concept by embedding phase-control strategies into trajectory-optimization frameworks, demonstrating noticeable reductions in community noise through dynamic phase-angle control. Pascioni et al. (Pascioni, Rizzi, & Schiller, 2019) provide additional insight into control requirements and indicate that a sound pressure level reduction of several decibels at the blade-passing frequency tone demands tight constraints on rotation-rate deviations.

These findings motivate the application of tailored synchronized distributed propellers for community and certification noise reduction in the context of urban air mobility (UAM). Despite acoustic and psychoacoustic investigations of the benefits of synchrophasing for simple propeller arrays, its psychoacoustic effect has not yet been widely studied for realistic distributed propulsion systems.

This acoustic effect does not apply only to propeller propulsion systems, but has already been demonstrated as a potential tonal noise-reduction mechanism for multistage compressors, known as “clocking”. Chen et al. (Chen, Gu, Xie, & Wang, 2006) experimentally investigate the impact of stator clocking on the performance of axial compressors with compound-lean stators in a low-speed, two-stage test facility. Their results show that compressor efficiency depends on the clocking position. A maximum efficiency increase of 1.22% at design conditions is achieved through the combined effects of compound-lean stator design and stator clocking. Kamiyoshi and Kaji (Kamiyoshi & Kaji, 2000) demonstrate tone-noise reduction in multistage fans through airfoil clocking. By combining rotor and stator clocking, they achieve more than $15\,\mathrm{dB}$ reduction at the blade passing frequency tone. Their findings indicate that sound-pressure levels can be minimized or even cancelled when rotor-blade and stator-vane settings are optimally adjusted. Milidonis et al. (Milidonis, Semlitsch, & Hynes, 2018) analyze the influence of stator clocking on compressor acoustic characteristics using high-fidelity and low-order numerical simulations of a 1.5-stage high-pressure compressor. They report that clocking has a negligible effect on compressor efficiency (less than 0.02%). However, it significantly modifies acoustic wave interference patterns in the near field.

These aeroacoustic studies indicate that synchrophasing can decrease tonal noise in multi-stage fan stages with only a slight or negligible impact on efficiency. However, to the best of the authors’ knowledge, it has not yet been investigated whether stator clocking can reduce tonal noise in distributed propulsion systems with ducted, single-stage fans.

This work first investigates whether sound quality improves using synchrophasing for a distributed propulsion system equipped with eight electrically driven propellers. The following research question is addressed: What tonal noise reduction potential and sound quality improvement can be achieved for distributed propellers under realistic UAM flight conditions? As a second step, we examine how synchrophasing can be applied to a distributed propulsion system equipped with 26 single-stage, ducted fans. Therefore, we ask the additional research question: Is it possible to adjust the stator positions of the individual fan stages (stator clocking) to reduce tonal noise in the distributed propulsion system? The hypothesis is formulated that, for low-count OGV fan engines, an optimal distribution of stator clocking positions exists in order to reduce tonal noise. For this purpose, an evolution-based optimization routine is employed to adjust the stator clocking angles of the 26 fan engines.

An auralization framework based on experimentally measured noise-emission data is employed to determine the noise signatures of the distributed propulsion systems. Experimental measurements under realistic conditions were performed in the Acoustic Wind tunnel Braunschweig (AWB) for the distributed propellers and in the Co-/Counter-Rotating Acoustic Fan Test rig (CRAFT) for the ducted fans. Several measurements are combined to represent the distributed propulsion systems for each UAM vehicle configuration. Virtual flyover simulations and binaural noise syntheses are then conducted to determine their noise signatures. As a post-processing step, sound quality metrics (SQMs) are calculated to assess the psychoacoustic characteristics of the noise signatures obtained.

This paper is organized as follows: Section 2 presents the considered distributed propulsion systems. Section 3 describes the methodology, with Sec. 3.1 summarizing the wind-tunnel propeller measurements, Sec. 3.2 summarizing the fan measurements, Sec. 3.3 showing the measurement-informed auralization framework, Sec. 3.4 describing the optimization process for the stator positions, and Sec. 3.5 describing the calculation of the SQMs. The results are presented and discussed in Sec. 4. The conclusions and outlook are formulated in Sec. 5.

2. UAM VEHICLES FOR AEROACOUSTIC STUDIES

The present study is based on two UAM vehicle concepts with distributed propulsion systems (Schade et al., 2026), illustrated in Fig. 1. Both concepts were developed within the VIRLWINT research program at the German Aerospace Center (DLR). The vehicles represent four-passenger electric vertical take-off and landing (eVTOL) aircraft. They are designed to enable detailed aeroacoustic investigations of distributed propulsion systems.

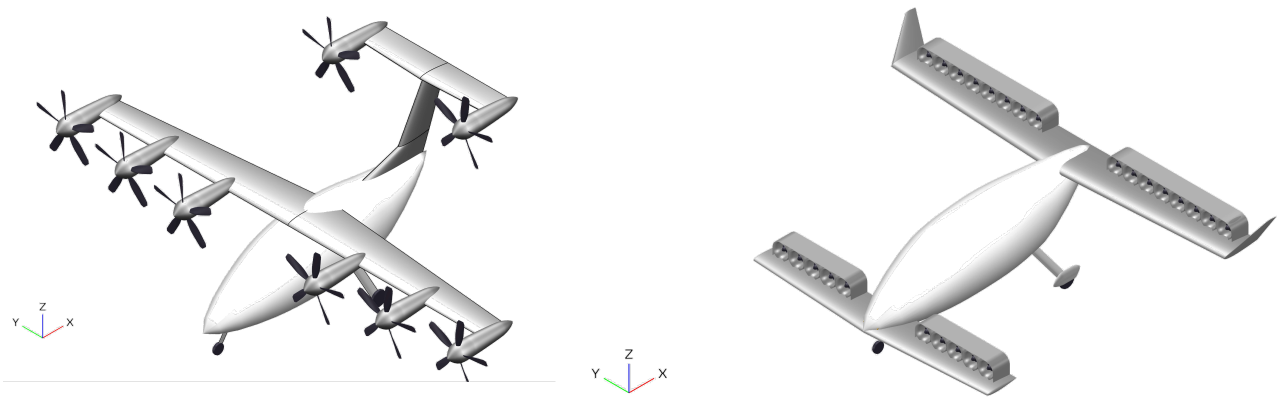

Figure 1: Tilt-prop (left) and tilt-duct (right) vehicle prototypes from project VIRLWINT designed for aeroacoustic studies.

Both vehicles share a common design point. This assumption ensures methodological consistency and enables a direct comparison of the two propulsion architectures. To design both vehicles, a hypothetical entry into service between 2030 and 2035 is assumed. The maximum payload is 450 kg, corresponding to four passengers and one pilot. The nominal cruise speed is 200 km/h and the maximum range is 150 km. A 20-minute loiter reserve is considered to account for operational safety margins.

The tilt-prop concept employs eight electrically driven open propellers distributed along the wings. The propeller diameter is 1.85 m. The cruise tip Mach number is 0.30.

The tilt-duct concept uses 26 ducted, tiltable fans mounted above the wings. Each fan has a diameter of 0.46 m. The design tip Mach number is 0.31.

3. METHODOLOGY

The propulsion systems of both aircraft concepts are considered to investigate the impact of synchrophasing on their noise signatures. The sound sources of the propulsion systems are based on measurement data. The overall study process is visualized in Fig. 2.

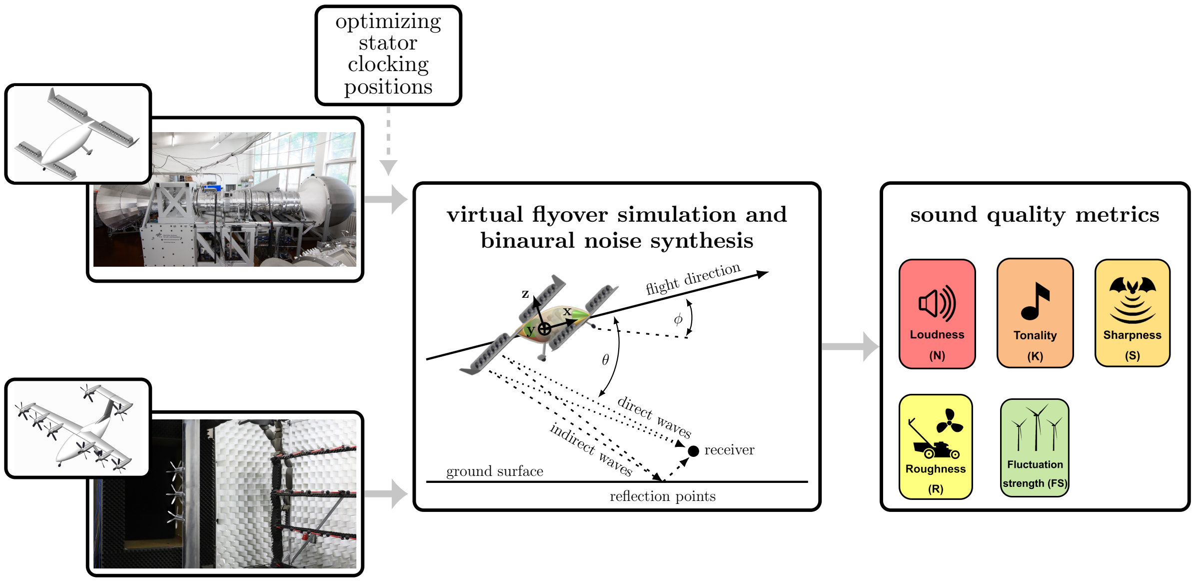

Figure 2: Process overview.

3.1 Propeller measurements

The measurement data presented in this contribution are the result of a close collaboration between DLR and Delft University of Technology (TU Delft). The wind tunnel model used in the experimental investigations consists of an array of three independently controllable propellers. The model was designed, fabricated, and operated by TU Delft. It features an unswept, untapered wing with NLF-Mod22(B) airfoil designed by Boermans and Rutten, characterized by a chord-length of 0.3 m and span of 1.248 m. For the AWB experiment, the effective span of the model is limited to the nozzle height of 1.2 m. The geometry of the three identical propellers used is the TUD-XPROP-S reference propeller, with a diameter of $D = 203.2$ mm and 6 blades with a pitch angle at 70% of the radius of $\beta_{0.7R} = 30$ degrees, and the axis of rotation angled 5 deg with respect to the wing chord line. Due to limitations of the electric motor, the propeller was restricted to an advance ratio of $J = 0.8$ at a wind tunnel velocity of 30 m/s, which would correspond to a thrust coefficient of $C_T = 1.05$ in isolated propeller conditions. A detailed presentation of the propeller rig has already been published elsewhere, and the interested reader may refer to (Duivenvoorden, Sinnige, & Veldhuis, 2025; De Vries, van Arnhem, Sinnige, Vos, & Veldhuis, 2021). The acoustic emissions, relevant for the results presented in this contribution, were acquired through a set of 36 Brüel and Kjær Type 4136 ¼” free-field microphones mounted in a planar fashion in a rectilinear grid arrangement in DLR’s Acoustic Wind Tunnel Braunschweig (AWB), see Fig. 3.

The considered microphone positions are selected to provide the widest possible spatial sampling of the emitted acoustic field. The acoustic signals, along with the $1/rev$ signal of all three propellers, are sampled at a 81 kHz rate on a GMB Viper GmbH 48-channel data acquisition unit for an acquisition duration of 60 seconds. An 88-microphone phased array mounted to the port side of the model was used in parallel with the free-field microphones to assess propeller wake-wing interaction effects.

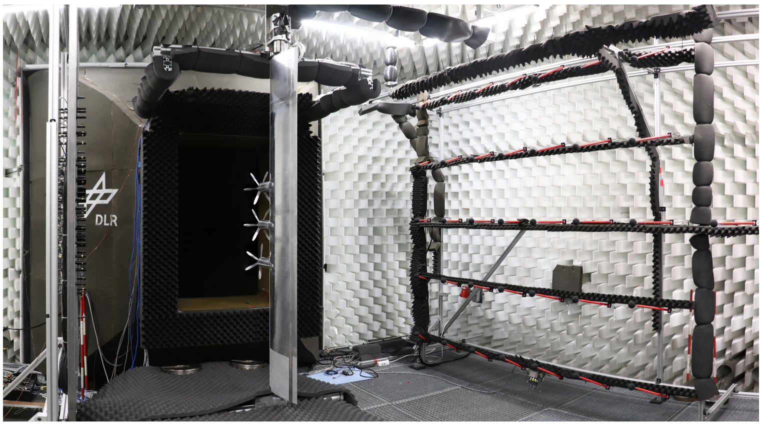

Figure 3: Experimental setup in the AWB. Left, phased microphone array. Right, free-field microphone grid. The wind tunnel model is the property of TU Delft and was kindly provided for the experiment.

3.2 Fan measurements

Measurements were conducted at the CRAFT (Co-/Contra Rotating Acoustic Fan Test) rig (see Fig. 4), described in (Tapken et al., 2021). The CRAFT rig features a modular two-shaft arrangement powered by two 45 kW motors. A long unsupported hub permits extensive acoustic measurements downstream of the fan.

Three fans were tested under clean-inflow conditions. However, since synchrophasing predominantly impacts tonal noise, a low-broadband fan stage was selected for the studies presented here (see Fig. 4). This fan is a low-count outer-guide-vane (OGV) design with 10 stator vanes and 31 rotor blades. The reduced number of stator vanes decreases broadband noise, leaving tonal components dominant. Consequently, the fan is well-suited for examining tonal interference effects caused by synchrophasing operation. The fan is operated at a rotational speed of $N = 4500$ rpm, a mass flow of $\dot{m} = 6.98$ kg/s and provides a pressure ratio of $\mathrm{PR} = 1.038$, and isentropic efficiency of $\eta_{ise} = 90.5$ %.

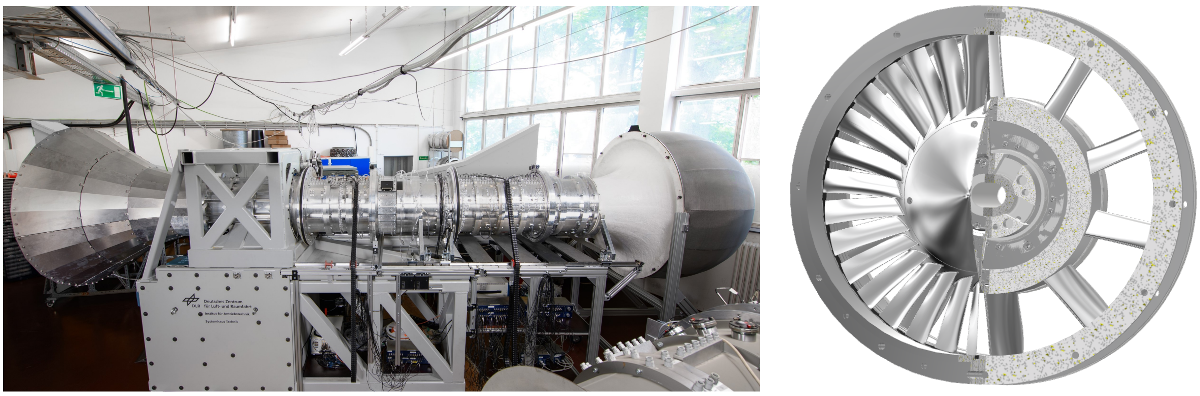

Figure 4: CRAFT test facility (left) and low-broadband fan stage (right).

Acoustic data were collected with flush-mounted G.R.A.S. condenser microphones (capsule 40BP, preamplifier 26AR). Thirty microphones were positioned along the inlet duct in a rotating duct section and spaced at a uniform axial distance of 23.75 mm. Twenty-two microphones were mounted similarly in the outlet duct. To resolve acoustic modes at the blade passing frequency (BPF) and its harmonics, measurements were taken at 59 circumferential positions. To determine the acoustic modes of the broadband sound field, two rings with 59 evenly spaced microphones were used, one upstream and one downstream of the fan.

Broadband mode amplitudes up to 6 kHz were obtained with a combined axial and azimuthal sensor array method (Tapken, Gutsche, & Enghardt, 2014). Above 6 kHz, only the ring array was used for an azimuthal mode analysis. The energy distribution among radial mode orders was calculated assuming equal energy per mode (Joseph, Morfey, & Lowis, 2003). In order to ensure continuity between the two analysis regimes, a weighted average of the methods was applied between 5 kHz and 6 kHz.

3.3 Measurement informed auralization framework

A measurement-informed auralization process transforms the acoustic measurement data from individual propulsion units into plausible, time-dependent sound signatures that can be used for psychoacoustic evaluation and design optimization.

The acoustic field around the propulsion units is provided as a hemispherical distribution of complex sound-pressure amplitudes over the azimuthal and polar angles at a fixed reference radius. These data capture the directional and frequency-dependent characteristics of the noise sources under the desired operating conditions.

The hemispheres containing the noise emission data are then processed using the tool VIOLIN (virtual acoustic flyover simulation) (Moreau et al., 2023) to propagate the engine-generated sound pressure amplitudes to ground-based microphones. The propagation is performed in the frequency domain. An interpolation step maps the measured sound pressure amplitudes from the hemispheres onto the time-varying emission angles of each engine. Because the source-receiver distance continuously changes during the flyover, a distance correction is applied to account for spherical spreading. Sound propagation through the atmosphere incorporates several atmospheric effects. The atmospheric absorption is calculated based on ISO 9613-1 (ISO 9613-1, 1993). Turbulent fluctuations are modeled according to Prescher et al. (Prescher, Moreau, & Schade, 2024), which introduce random amplitude and phase modulations that manifest as vertical stripes in the spectrograms. The Doppler frequency shift is applied to account for the relative motion of source and receiver. The ground is treated as an ideal acoustically hard surface (ground flow resistivity $\sigma \rightarrow \inf$). The attenuation and reflection of indirect sound waves are modeled according to (Arbeitsgruppe Novellierung der AzB, 2007). Indirect waves acquire a phase shift that depends on the travel-distance difference between the direct and indirect propagation paths. This phase shift is incorporated into the propagation calculation for each engine and each noise source. The direct and reflected sound waves are then summed to obtain the total sound pressure amplitudes at the receiver position for each engine and source. This superposition results in constructive and destructive interference patterns that manifest as U-shaped stripes visible in the spectrograms.

Virtual flyover simulations are conducted for both propulsion systems: distributed fans and distributed propellers. Identical trajectory and environmental parameters are applied to both cases. The flight path follows the EASA reference procedure for tilting-rotor VTOL aircraft (EASA, 2023). The procedure specifies a horizontal overflight at an altitude of 150 m. A central microphone is positioned directly beneath the trajectory at a height of 1.2 m. The aircraft operates at a flight Mach number of $M_{\text{flight}} = 0.16$. The angle of attack is fixed at $3\ \text{deg}$. Environmental conditions are defined according to the EASA standard (EASA, 2023). Atmospheric pressure is $p_0 = 101{,}325$ Pa. The ambient temperature is $T_0 = 15\ \text{deg}$C. Relative humidity is maintained at 70 %.

Finally, the resulting time- and frequency-dependent spectrograms are converted into binaural audio files using the tool CORAL (aircraft engine noise auralization) (Moreau et al., 2023). The binaural audio files are generated by convolving the monaural time series with head-related impulse responses (HRIRs). Artificial HRIRs, measured by Bernschütz (Bernschütz, 2013), are used to ensure consistency and avoid subject-specific variations. The final output is a set of WAV files that can be used as stimuli in listening experiments or for further analysis.

3.4 Optimization process for stator clocking positions

In order to examine how synchrophasing can be applied to the distributed propulsion system equipped with 26 single-stage, ducted fans, an optimization process is applied. The idea is to find an optimized stator clocking angle distribution for the 26 fan stages in order to reduce tonal noise due to destructive interference. Stator clocking, consisting of adjusting the relative circumferential position of stators in adjacent fan stages, has the potential to decrease the tonal noise emission of the distributed propulsion system. Tonal noise constitutes an interaction noise source. It results from the interaction between rotor wakes and the downstream stator leading edge. Periodic wake impingement induces unsteady pressure fluctuations, which cause a variation of airfoil lift. An acoustic dipole is generated at the stator leading edge. With different stator clocking angles between the 26 fan stages, the tonal noise generation exhibits a phase shift between adjacent engines. In good approximation, tonal acoustic noise sources can be treated as fully correlated. Therefore, due to phase differences, for distributed propulsion systems whose noise signature is dominated by tones, interference between the acoustic waves emitted by each engine can generate strong variations in the directivity pattern. Thus, the hypothesis is formulated that an optimal stator clocking angle distribution exists, which results in destructive interference and, therefore, reduces tonal noise emission. Thereby, it is assumed that the measured directivity of one single fan does not change due to the modification of the stator clocking position.

It is reasonable to optimize the stator clocking angles instead of those of the rotors since the stator mounting positions can be controlled by design. Stators are fixed components. Rotors, however, allow for angular deviation. Consequently, the rotor clocking angles may vary during operation. For the present optimization, a fixed, random angle distribution is applied to the 26 rotors. The impact of different rotor angle distributions on the optimized stator angle distribution is out of scope for this study.

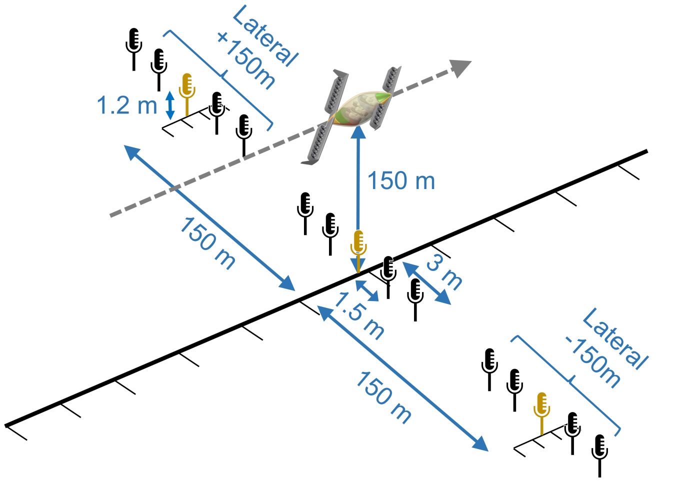

Figure 5: Overview of the selected observer locations, including those recommended by EASA (highlighted in yellow).

The 26-dimensional objective function exhibits high complexity and numerous local minima. Consequently, the SciPy Differential Evolution (DE) is selected as the optimization strategy (Virtanen, Gommers, & Oliphant, 2020). This algorithm effectively mitigates the risk of premature convergence within local optima. To ensure physical feasibility, the stator clocking angles are restricted to integer values. This prevents the algorithm from converging to unrealistically precise solutions. The ”best1bin“ mutation strategy is employed. The optimization process converged after approximately 300 iterations.

The optimization is performed with the tool VIOLIN. The tonal noise emission of the distributed propulsion system is optimized. The considered trajectory is visualized in Fig. 5. The virtual flyover is performed for a simulation time of $15\,\mathrm{s}$. Within the optimization procedure, the tonal noise emission is propagated to 15 microphones. Each microphone has a height of $1.2\,\mathrm{m}$. The 15 microphones considered are clustered around the certification microphones, which are highlighted in yellow in Fig. 5. Thus, three microphone corridors, each containing five microphones with a microphone distance of $1.5\,\mathrm{m}$, are considered: one centerline corridor, two lateral at $+150\,\mathrm{m}$, and $-150\,\mathrm{m}$ (see Fig. 5). This setup ensures that tonal noise levels are minimized at the certification microphones as well as in their direct vicinity. Optimizing within these corridors addresses two practical limitations. First, it prevents the selection of mathematically optimal but impractically precise solutions. Second, it accounts for realistic flyover conditions, since actual aircraft trajectories may deviate from idealized straight paths.

Differential Evolution requires a scalar objective function. Consequently, acoustic data from the three corridors (in total 15 microphones) must be aggregated into a single metric. Each microphone corridor is evaluated independently. The corridor-specific objective function combines the mean and standard deviation and is defined as follows:

$$\mathrm{cost}_{\mathrm{corridor}} = a_1\, Mean + 5\, a_2\, Std, \tag{1}$$

where $\mathrm{cost}_{\mathrm{corridor}}$ is calculated using the five microphones in each of the three corridors (see Fig. 5). The coefficients are specified as $a_1 = 1$ and $a_2 = 0.7$. These coefficients were determined iteratively. This weighting prioritizes the mean term over the standard deviation. The factor of 5 compensates for the magnitude discrepancy. Afterwards, the cost functions from each corridor are summed:

$$\mathrm{cost} = \mathrm{cost}_{\mathrm{Lateral}+150m} + \mathrm{cost}_{\mathrm{Centerline}} + \mathrm{cost}_{\mathrm{Lateral}-150m} \tag{2}$$

The mean function minimizes the overall acoustic levels. The standard deviation function promotes spatial uniformity, which is expected to benefit the SQMs, as well as real-life deviations from the expected certification trajectory.

3.5 Sound quality assessment

On top of conventional sound metrics typically used in noise assessment, such as the maximum sound pressure level $\mathrm{L}_{\mathrm{p,max}}$ or the effective perceived noise level (EPNL), the sound quality assessment is performed using sound quality metrics (SQMs) and psychoacoustic annoyance (PA) models that combine multiple SQMs. The SQMs describe the subjective perception of sound by human hearing, unlike the sound pressure level, which quantifies the purely physical magnitude of sound based on pressure fluctuations. Previous studies (Merino-Martinez, Pieren, & Schäffer, 2021; Merino-Martinez, Yupa-Villanueva, von den Hoff, & Pockelé, 2024; Merino-Martinez & Buzetelu, 2025) showed that these metrics better capture the auditory behavior of the human ear compared to conventional sound metrics typically employed in noise evaluations. The five most commonly used SQMs (Greco, Merino-Martinez, Osses, & Langer, 2023) are:

- Loudness (N): Subjective perception of sound magnitude of the overall sound intensity. Two models are considered in this study: Zwicker's ISO 532-1 model (*ISO norm 532–1 – Acoustics – Method for calculating loudness – Zwicker method*, 2017) and Sottek's ECMA 418-2:2025 model (Ecma International, 2025). The unit of this metric is sone[1].

[1] For the metrics corresponding to Sottek's ECMA 418-2:2025 model, the subindex HMS is added to denote that they refer to the Hearing Model Sottek.

- Tonality (K): Measurement of the perceived strength of unmasked tonal energy within a complex sound. Two models are considered in this study: Aures' (Aures, 1985) and Sottek's ECMA 418-2:2025 (Ecma International, 2025). The unit of this metric is tonality unit (t.u.).
- Sharpness (S): Representation of the high-frequency sound content. In this study, the model by von Bismark is employed (von Bismark, 1974). The unit of this metric is acum.
- Roughness (R): Hearing sensation caused by sounds with modulation frequencies between 15 Hz and 300 Hz. The model by Daniel and Webber (Daniel & Webber, 1997) is used, and the unit of this metric is asper.
- Fluctuation strength (FS): Assessment of slow fluctuations in loudness with modulation frequencies up to 20 Hz, with maximum sensitivity for modulation frequencies around 4 Hz. The model by Osses et al. (Osses, García León, & Kohlrausch, 2016) is considered here, and the unit of this metric is vacil.

The SQMs are expressed using the 5%-exceeded value (i.e., the 95$^{\text{th}}$ percentile) for each signal. This representative value is selected based on common practice in the literature, where the 95$^{\text{th}}$ percentile is often used to describe sound quality metrics, following the recommendation originally proposed by Fastl and Zwicker (Fastl & Zwicker, 2007). The PA models proposed by More (More & Davies, 2010) and Di et al. (Di, Chen, Song, Zhou, & Pei, 2016) are used in this work, which combine the 5%-exceeded values of the five SQMs mentioned above into a single global metric. All the conventional sound metrics, SQMs, and the PA metrics were computed using the open-source MATLAB toolbox SQAT (Sound Quality Analysis Toolbox) v1.3 (Greco, G. F. and Merino-Martinez, R. and Osses, A. and Lotinga, M.J.B., 2025).

In order to help evaluate the variations in individual SQMs obtained by the different configurations considered (i.e. different synchrophasing settings), the just-noticeable difference (JND) values per SQM (taken from (Osses, Greco, & Merino-Martinez, 2023)) are presented in the results section (see Fig. 10). This evaluation follows the hypothesis that sounds that differ by more than one JND are perceived as significantly different from each other.

4. Results and Discussion

In this section, the results are presented and discussed. In Sec. 4.1, it is first investigated whether sound quality improves using synchrophasing for the distributed propulsion system equipped with eight electrically driven propellers. The research question "*What tonal noise reduction potential and sound quality improvement can be achieved for distributed propellers under realistic UAM flight conditions?*" is addressed. As a second step, in Sec. 4.2, it is examined how synchrophasing can be applied to the distributed propulsion system equipped with 26 single-stage, ducted fans. The optimization procedure, outlined in Sec. 3.3, is applied to the 26 stator clocking angles in order to find an optimum clocking angle distribution for tonal noise reduction.

4.1 Synchrophasing for distributed propellers

Figure 6 shows the spectrograms of the distributed propellers at the central microphone for $\mathrm{AOA} = 0\,\mathrm{deg}$ and different $\Delta\phi$ values. Due to the propeller full-scale diameter of $1.85\,\mathrm{m}$ (i.e. about 9 times larger than the ones tested at AWB, see section 3.1), the propeller operates at a relatively low rotational speed. Thus, the propeller tones are visible in the spectrograms at low frequencies below $800\,\text{Hz}$. The BPF tone is visible at $120\,\text{Hz}$ and 15 of its harmonics are included in the auralization, whereas most of the higher harmonics are masked by broadband noise in the present case. Measurements are conducted on model-scale propellers, which inherently limit the measurable maximum frequency. Consequently, the sharp boundary observed in the upper-right corner of the spectrograms is not a physical phenomenon but rather an artifact arising from the absence of measurement data at higher frequencies.

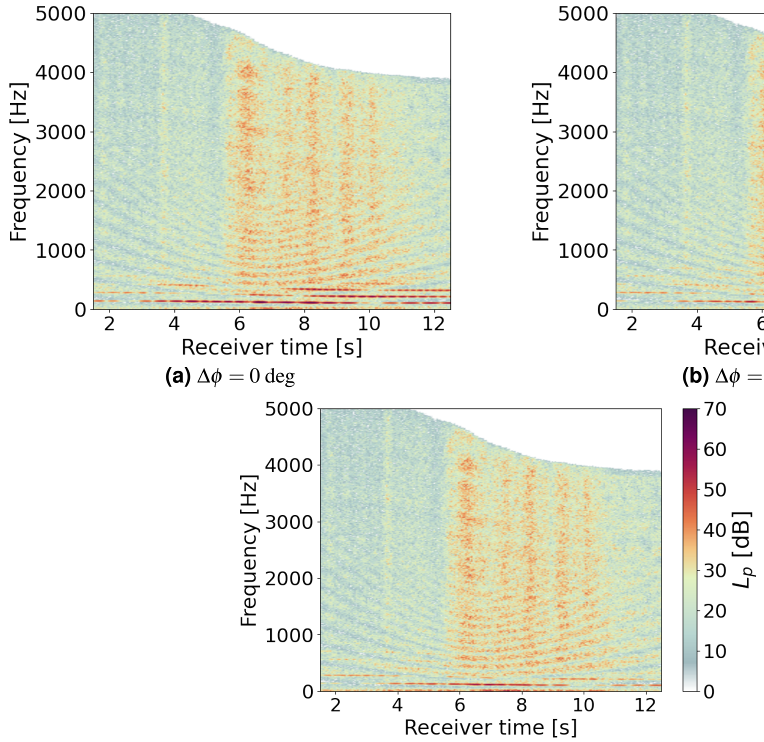

(a) $\Delta\phi = 0\,\text{deg}$ **(b)** $\Delta\phi = 30\,\text{deg}$ **(c)** $\Delta\phi = \text{random}$

Figure 6: Spectrograms for the distributed propellers at the central microphone and $\text{AOA} = 0\,\text{deg}$ for different $\Delta\phi$.

Measurements are performed with $\Delta\phi = 0, 10, 30\,\text{deg}$ and $\Delta\phi = \text{random}$. With $\Delta\phi = 30\,\text{deg}$ and $\Delta\phi = \text{random}$, a significant noise level reduction of the BPF tone and its harmonics is achieved compared to $\Delta\phi = 0\,\text{deg}$. This reduction results from destructive interference effects due to the different relative blade angles between adjacent propellers. These destructive interferences manifest as an amplitude reduction and lead to temporal tonal amplitude modulations. Since a 6-bladed propeller is used for the measurements, $\Delta\phi = 30\,\text{deg}$ is equivalent to half the propeller blade-to-blade angle.

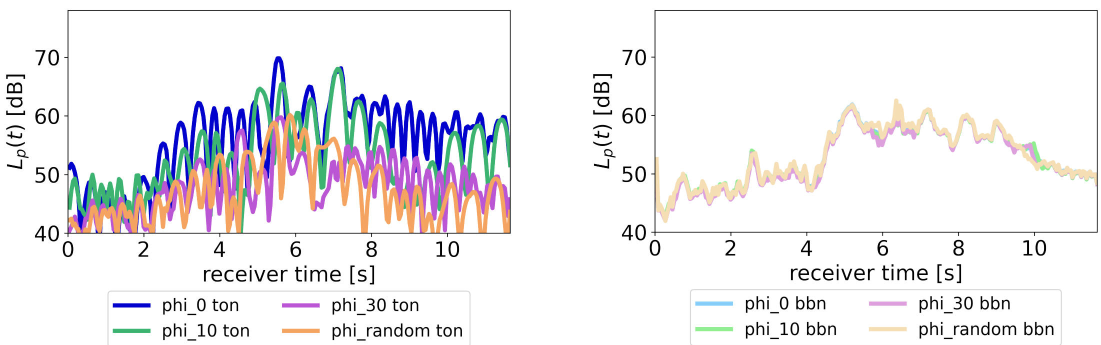

(a) Tonal time signals **(b)** Broadband time signals

Figure 7: Tonal and broadband time signals for the distributed propellers at the central microphone and $\text{AOA} = 0\,\text{deg}$ for different $\Delta\phi$ values.

Figure 7 shows the tonal (see Fig. 7a) and broadband (see Fig. 7b) time signals of the distributed propellers at the central microphone for $\mathrm{AOA} = 0\,\mathrm{deg}$ and different $\Delta\phi$ values. As expected, due to the stochastic and incoherent character of broadband noise, modifying the relative blade-phase angle $\Delta\phi$ has no mitigating effect, as visualized in Fig. 7b. For tonal noise, increasing the relative blade-phase angle results in a continuous reduction in sound pressure level, with the largest reduction of ≈ 10 dB occurring at $\Delta\phi = 30\,\mathrm{deg}$. Interestingly, with a random distribution of the blade-phase angles, a reduction in the tonal sound pressure level similar to that achieved for $\Delta\phi = 30\,\mathrm{deg}$ is obtained. However, it should be noted that only one random distribution was set in the experiment. It is, therefore, possible that other settings for "random" exist, for which no reduction, or a smaller reduction, in the sound pressure level is achieved.

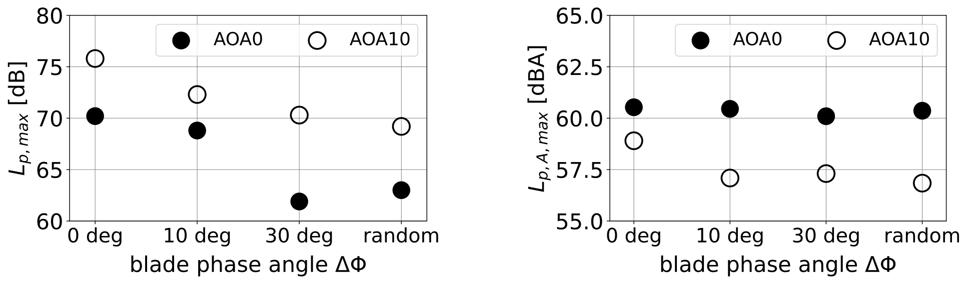

Figure 8: Comparison between maximum sound pressure level $L_{\mathrm{p,max}}$ (left) and maximum A-weighted sound pressure level $L_{\mathrm{p,A,max}}$ (right) for the case with distributed propellers.

Figure 8 presents the maximum overall sound pressure level $L_{\mathrm{p,max}}$ and the maximum A-weighted sound pressure level $L_{\mathrm{p,A,max}}$ as a function of the relative blade-phase angle $\Delta\phi$ for two angle-of-attack conditions ($\mathrm{AOA} = 0\,\mathrm{deg}$ and $\mathrm{AOA} = 10\,\mathrm{deg}$). For $\mathrm{AOA} = 0\,\mathrm{deg}$, a pronounced reduction in $L_{\mathrm{p,max}}$ is observed at $\Delta\phi = 30\,\mathrm{deg}$, consistent with the expected destructive interference at half the blade-to-blade angle for a six-bladed propeller, as reported by Monteiro et al. (d. Monteiro et al., 2024). The $\mathrm{AOA} = 10\,\mathrm{deg}$ condition exhibits a comparatively more modest sensitivity to $\Delta\phi$, suggesting that inflow distortion induced by the angle of attack partially disrupts the phase coherence required for effective tonal cancellation. The A-weighted levels in $L_{\mathrm{p,A,max}}$ follow qualitatively similar trends, although the absolute reductions are attenuated relative to the unweighted levels, reflecting the lower contribution of low-frequency tonal components after A-weighting. It is also worth noting that once A-weighting is applied, the noise levels for $\mathrm{AOA} = 0\,\mathrm{deg}$ are higher than those for $\mathrm{AOA} = 10\,\mathrm{deg}$, unlike for the unweighted case.

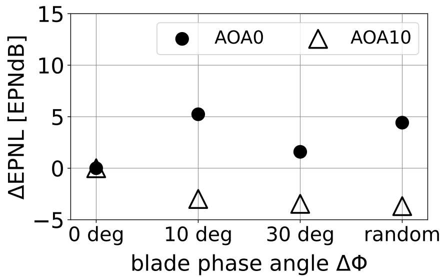

Figure 9: Difference in the effective perceived noise level (ΔEPNL) relative to $\Delta\phi = 0\,\mathrm{deg}$ for the case with distributed propellers.

The differences in Effective Perceived Noise Level (ΔEPNL) relative to the reference condition $\Delta\phi = 0\,\mathrm{deg}$ are shown in Fig. 9. For $\mathrm{AOA} = 10\,\mathrm{deg}$, all the cases with $\Delta\phi \neq 0\,\mathrm{deg}$ yield consistent reductions in EPNL or roughly 3 EPNdB, whereas the $\mathrm{AOA} = 0\,\mathrm{deg}$ setting shows EPNL increases relative to the reference case. This fact may appear counterintuitive, but it may be attributed to the spectral redistribution of the tonal energy rather than its reduction, since the EPNL metric does account for the presence of tones in a limited manner. These EPNL variations also underscore the directivity-dependent nature of synchrophasing benefits, as the EPNL metric integrates the perceived noise over the duration of the flyover event, whereas the results from Fig. 8 only considered the maximum values.

Figure 10 presents the results for the five SQMs introduced in section 3.5, with error bars denoting the JND thresholds.

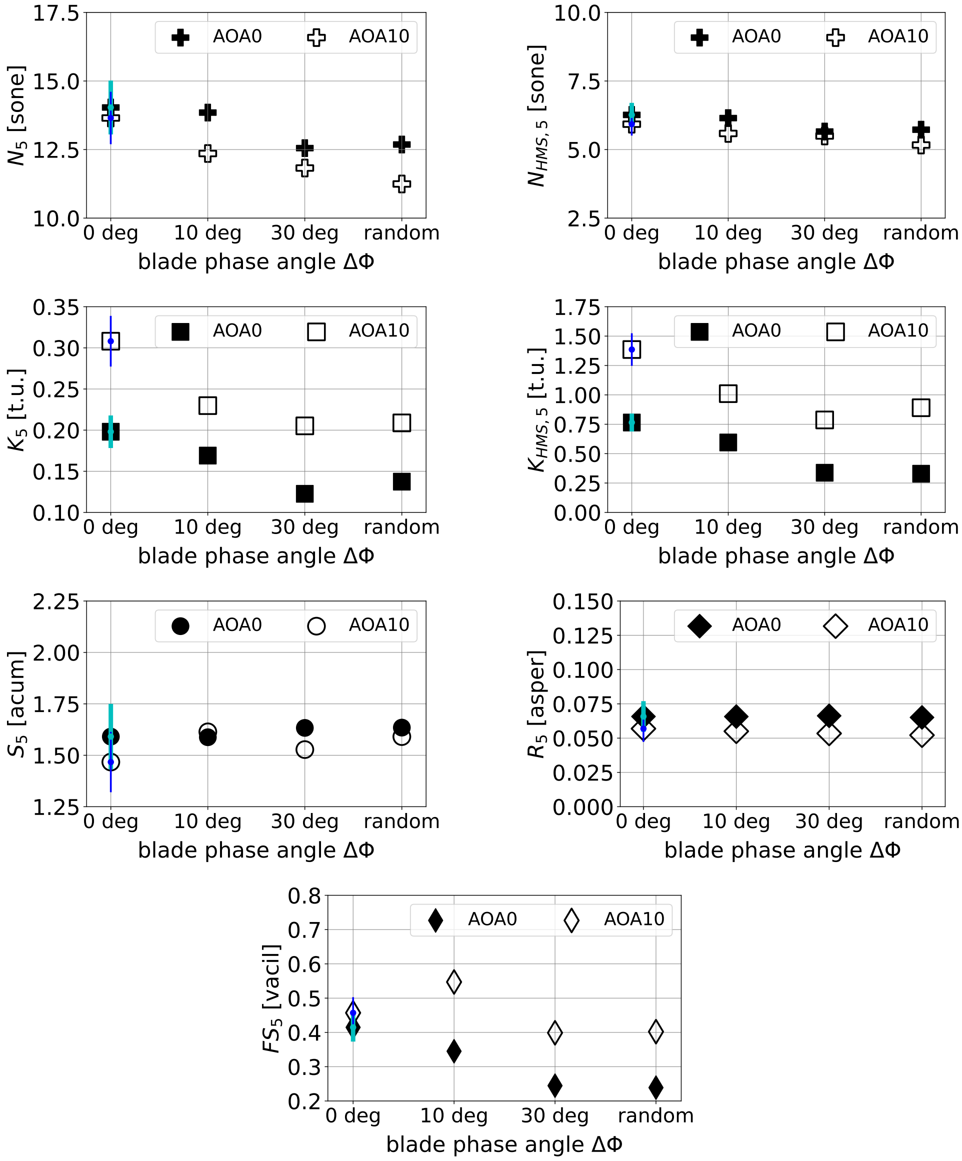

Figure 10: Sound quality metrics for the case with distributed propellers. The error bars refer to the JNDs, where each error bar is plotted as ±JND.

For loudness, the Zwicker model indicates modest reductions in loudness with increasing $\Delta\phi$ for $\mathrm{AOA} = 0\,\mathrm{deg}$, with the most pronounced decrease at $\Delta\phi = 30\,\mathrm{deg}$. For $\mathrm{AOA} = 10\,\mathrm{deg}$, the reductions become more noticeable and are all larger than the JND threshold. For the HMS case, the same trends are observed, although with relatively smaller variations. For both models and for $\mathrm{AOA} = 10\,\mathrm{deg}$, the random case seems to provide the largest loudness reductions.

The tonality metrics exhibit substantial and consistent reductions across synchrophasing conditions for $\mathrm{AOA} = 0\,\mathrm{deg}$, with $\Delta\phi = 30\,\mathrm{deg}$ and the random phase case yielding the largest reductions that exceed one JND threshold compared to the $\Delta\phi = 0\,\mathrm{deg}$ baseline. This is physically expected, as synchrophasing targets tonal noise primarily through destructive interference at the blade-passing frequency and its harmonics. In general, the HMS values show a larger dynamic range compared to those from the Aures model, suggesting greater sensitivity of the former to the tonal structure of the signal. In general, the $\mathrm{AOA} = 10\,\mathrm{deg}$ condition exhibits higher absolute tonality values across all phase angles.

Sharpness remains roughly invariant across all synchrophasing conditions for both AOA cases, with variations remaining well within one JND. This is consistent with the fact that sharpness is predominantly governed by high-frequency spectral content, which is not directly targeted by synchrophasing-induced tonal interference.

Similarly, all roughness values appear to be stable across $\Delta\phi$ configurations, with no statistically meaningful trends discernible beyond the JND. Since roughness is associated with amplitude modulations in the $15-300$ Hz range, and synchrophasing primarily modifies steady-state tonal amplitudes rather than modulation depth, this result is physically plausible.

A more notable variation is observed in fluctuation strength, particularly for $\mathrm{AOA} = 0\,\mathrm{deg}$, which presents reductions considerably beyond the JND. Interestingly, for the $\mathrm{AOA} = 10\,\mathrm{deg}$ configuration and the case with $\Delta\phi = 10\,\mathrm{deg}$, a substantial increase in fluctuation strength is observed compared to the baseline. The exact reasons for this, however, remain unknown.

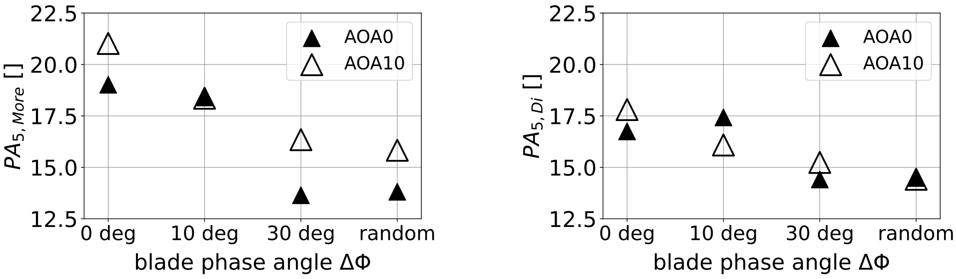

Figure 11: Comparison of psychoacoustic annoyance values determined with the models developed by More (More & Davies, 2010) (left) and Di et al. (Di et al., 2016) (right) for the case with distributed propellers.

The composite psychoacoustic annoyance values from the models by More and Di et al. are presented in Fig. 11. Both models yield qualitatively consistent trends: Overall, $\mathrm{AOA} = 0\,\mathrm{deg}$ benefits most from synchrophasing, with the lowest PA values achieved at $\Delta\phi = 30\,\mathrm{deg}$, broadly corroborating the trends in tonality reduction observed in Fig. 10. The $\mathrm{AOA} = 10\,\mathrm{deg}$ condition produces, in general, higher absolute PA values at $\Delta\phi = 0\,\mathrm{deg}$, but shows a monotonically decreasing trend with increasing blade-phase angle, converging toward similar PA levels as $\mathrm{AOA} = 0\,\mathrm{deg}$ at $\Delta\phi = 30\,\mathrm{deg}$, and the random case for the PA model by Di et al. . A main difference between the two PA models considered in this study is how they evaluate the tonal prominence and overall tonality in the psychoacoustic annoyance computation. For this particular scenario, More's model seems to be more sensitive to the variations caused by the differences in blade-phase angle.

Overall, Figures 8 to 11 collectively demonstrate that synchrophasing at $\Delta\phi = 30\,\mathrm{deg}$, yields the most consistent improvements across physical and psychoacoustic metrics for $\mathrm{AOA} = 0\,\mathrm{deg}$, with tonality emerging as the metric most responsive to phase optimization. The benefits are more nuanced under $\mathrm{AOA} = 10\,\mathrm{deg}$ inflow conditions, highlighting the sensitivity of synchrophasing effectiveness to the aeroacoustic operating environment.

4.2 Synchrophasing for distributed ducted fans

Figure 12 illustrates the instantaneous tonal noise footprints of the distributed ducted fan propulsion system. The results correspond to the reference (Fig. 12a), the worst (Fig. 12b) and the best (Fig. 12c) stator clocking angle distributions. Since the optimization procedure is not explicitly designed to target global maxima, it should be noted that there may exist stator angle distributions resulting in even higher tonal noise levels than the worst-case scenario depicted. As a reference case, an identical stator clocking distribution is considered, which corresponds to $\Delta\phi = 0\,\mathrm{deg}$. In this case, the stator vanes of all 26 fan stages are mounted in the same position. Each plot can be interpreted as a temporal snapshot of the tonal noise immission on the ground during a flyover. To obtain these results, the center of gravity of the distributed propulsion system is placed at a fixed position at an altitude of $150\,\mathrm{m}$ and $(X,Y) = (0,0)$ and the fan stages are distributed spatially according to Fig. 1. The tonal noise is then propagated to ground-based microphones at a height of $1.2\,\mathrm{m}$.

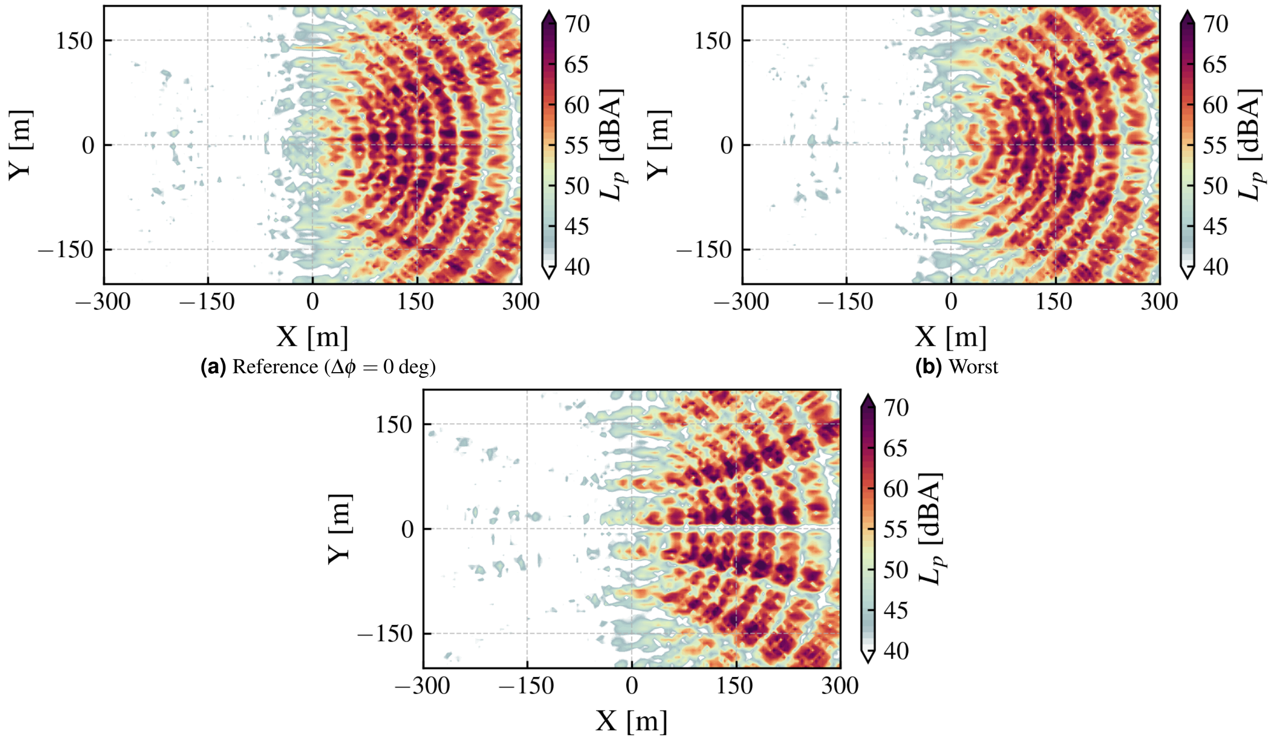

Figure 12: Instantaneous tonal noise footprint of the distributed ducted fans for different stator clocking angle distributions.

The low-broadband fan stages predominantly radiate tonal noise upstream (see $X > 0\,\mathrm{m}$). In addition, the tonal noise footprint is significantly affected by interference effects, manifesting as a complex wave-like and striped pattern. The wave-like structures result from the ground reflection from the superposition of the direct and reflected sound waves. The reference stator angle distribution and the worst-case scenario of the optimization yield qualitatively nearly identical results, whereby the tonal noise levels are slightly higher overall in the worst-case scenario. The optimization yields a considerable reduction in tonal noise levels, particularly within the centerline microphone corridor, resulting in a narrow low-tonal noise area around the centerline.

For noise certification at a centerline microphone, the optimization method identified a stator angle distribution that significantly reduces tonal noise levels directly below the aircraft (in the vicinity of the centerline). This establishes the stator angle distribution as a new design degree of freedom for developing low-noise distributed propulsion systems. However, this result also introduces a potential drawback. The results indicate that optimizing the stator angle distribution may create a localized low-tonal-noise corridor directly below the aircraft. While this reduces centerline certification noise, it does not necessarily lower sound exposure for surrounding communities, such as airport residents, at the lateral emission angles. Although with the optimized stator angle distribution slightly lower lateral tonal noise levels are obtained, additional low-noise corridors like the one in the vicinity of the centerline cannot be achieved.

Figure 13 shows the temporal evolution of the A-weighted tonal and broadband sound pressure levels for the distributed ducted fan propulsion system for a horizontal flight path at an altitude of $150\,\mathrm{m}$. The results correspond to the reference (top), the worst (middle) and the best (bottom) stator clocking angle distribution. The time signals are plotted for the three certification microphones (highlighted in yellow in Fig. 5): the lateral microphones in the left and right columns and the centerline microphone in the center column. The vertical dashed lines show the receiver times when the microphones are passed.

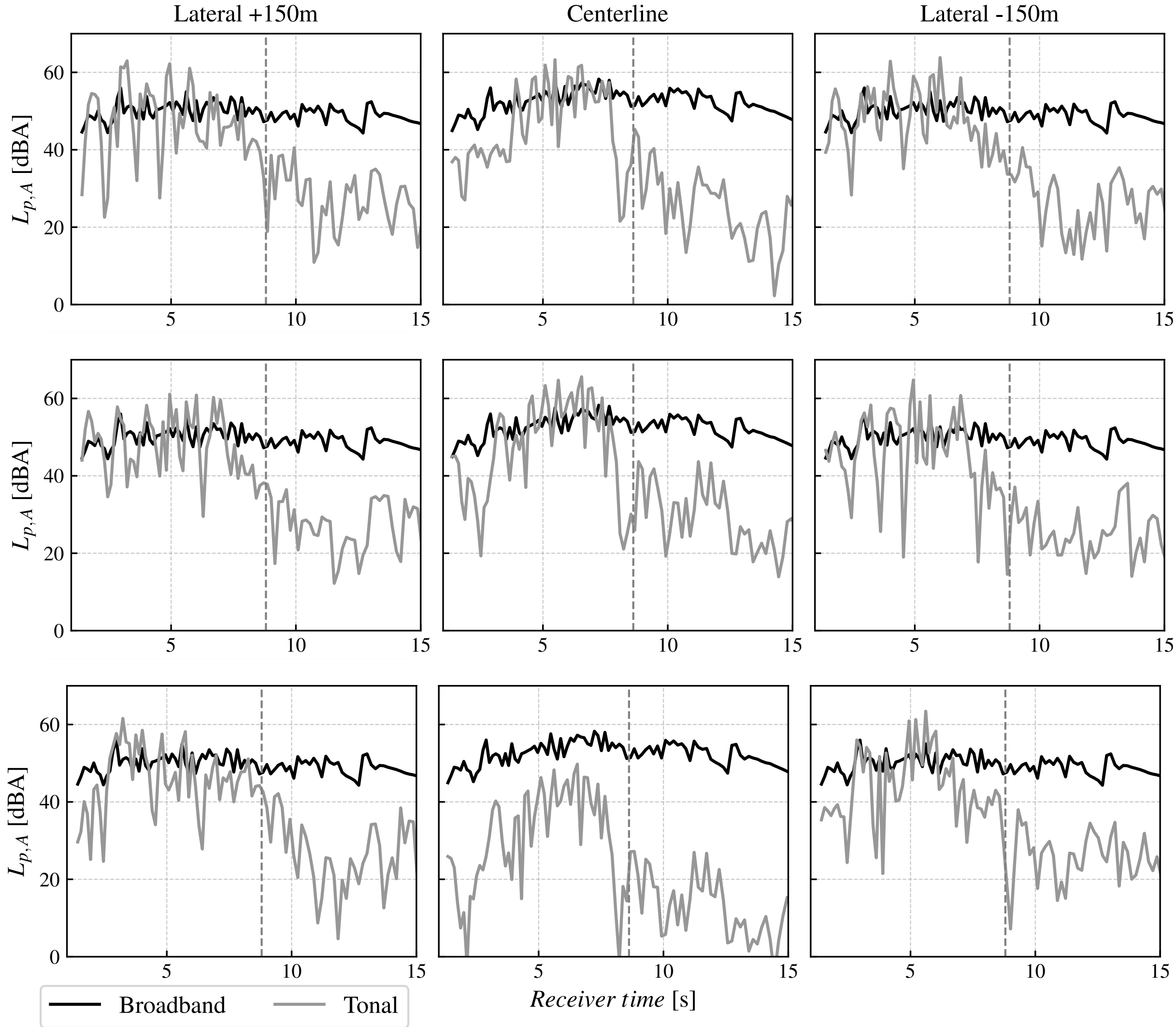

Figure 13: A-weighted sound pressure levels for the distributed ducted fans at the three certification microphones for different stator clocking angle distributions. The vertical, dashed lines indicate the time when the microphone is passed. Top: Reference stator clocking angle distribution; middle: Worst stator clocking angle distribution; Bottom: Best stator clocking angle distribution.

With the reference and worst-case stator angle distributions, the A-weighted tonal noise levels exceed the broadband levels before the microphone is passed (see $0 < t < 7\,\mathrm{s}$). The sudden drop in tonal levels after the microphone is passed results from the acoustic design of the low-broadband fan stages (see Schade et al. (Schade, Jaron, Klähn, & Moreau, 2024)). With the optimized stator angle distribution, a considerable reduction in tonal noise levels is achieved, especially at the centerline. For the centerline microphone, the tonal noise levels are reduced by $10\,\mathrm{dBA}$ compared to the reference and worst-case scenarios, resulting in the tonal levels being masked by the broadband levels during all times of the flyover. At the lateral microphone positions, the reduction in tonal noise is less pronounced. Nevertheless, at both lateral locations, the time span during which tonal levels exceed broadband levels is shortened. For instance, at the $-150\,\mathrm{m}$ lateral microphone, tonal noise exceeds broadband noise over the time period $1.5 < t < 7\,\mathrm{s}$ for the reference and worst-case scenarios. However, with the optimized stator angles distribution, this interval decreases to $4.8 < t < 6\,\mathrm{s}$.

5. Summary and conclusion

This study investigated the acoustic and psychoacoustic potential of active interference-based noise control strategies for distributed electric propulsion systems in urban air mobility (UAM) applications. The work addressed two research questions: first, what tonal noise reduction potential and sound quality improvement can be achieved using synchrophasing for distributed propellers under realistic UAM flight conditions; and second, whether adjusting the stator positions of single-stage fans (stator clocking) can reduce tonal emissions across a ducted fan array.

For the eight-propeller distributed propulsion system, synchrophasing proved effective under realistic UAM conditions. The largest reductions were achieved at a relative blade-phase angle of $\Delta\phi = 30\,\mathrm{deg}$, which corresponds to half the blade-to-blade angle for the six-bladed propellers. Physically, this specific phase shift induces destructive interference at the blade-passing frequency and its harmonics, yielding tonal sound pressure level reductions of approximately $10\,$dB compared to the in-phase baseline. The corresponding sound quality metrics (SQMs) corroborate these findings: tonality decreases substantially, exceeding one just-noticeable difference (JND) threshold for both standard and hearing-model-based assessments. Fluctuation strength also shows marked improvements, while loudness reductions are more modest. Sharpness and roughness remain largely invariant across all phase settings, as these metrics depend on high-frequency spectral content and mid-frequency amplitude modulations, respectively, which are not directly targeted by phase control, which impacts the low-frequency propeller tones.

For the 26 distributed fans, an evolution-based optimization routine was employed to determine an optimal stator clocking angle distribution across the 26 engines targeting tonal noise reduction. The optimized distribution successfully creates destructive interference across the fan array. At the certification centerline microphone, this configuration reduces tonal noise levels by approximately $10\,$dBA relative to reference and worst-case scenarios. While lateral reductions are less pronounced, the time span during which tonal noise dominates is significantly shortened. While the stator angle optimization effectively reduced centerline tonal noise through targeted acoustic interference, leading to a low-tonal noise corridor beneath the flight path, a broader reduction of community noise could not be achieved.

In conclusion, both synchrophasing for open propellers and stator clocking for ducted fans offer viable pathways for tonal noise mitigation in distributed propulsion systems. Phase control delivers consistent psychoacoustic improvements under ideal flight conditions, while stator clocking optimization provides targeted centerline noise reduction for single-stage fan arrays. Regarding stator clocking, future work should focus on mitigating the trade-off between localized, low-noise certification corridors and a broader community noise reduction. In general, these findings should also be validated with perceptual listening experiments to evaluate potential reductions in reported noise annoyance.

Acknowledgments

This publication is part of the project *VIRLWINT* (Virtual acoustical twin of distributed propulsion systems) funded by the German Aerospace Center (DLR).

The authors also gratefully acknowledge funding by the Deutsche Forschungsgemeinschaft (DFG, German Research Foundation) under Germany´s Excellence Strategy – EXC 2163/1 - Sustainable and Energy Efficient Aviation – Project-ID 390881007.

The wind tunnel measurements presented herein are a joint effort by DLR and TU Delft. The authors also acknowledge the expertise and efforts provide by Buğrahan Öztürk and Fernanda do Nascimento Monteiro in the preparation and conduction of the experiment with the distributed propeller wind tunnel model of TU Delft.

The work of Roberto Merino-Martínez is part of the project *Listen to the future* (with project number 20247) of the research programme Veni 2022 (Domain Applied and Engineering Sciences), which is (partly) financed by the Dutch Research Council (NWO).

References

Arbeitsgruppe Novellierung der AzB. (2007, 05). Anleitung zur Berechnung von Lärmschutzbereichen (AzB). *Umweltbundesamt*.

Attenuation of sound during propagation outdoors, part 1: Calculation of the absorption of sound by the atmosphere (norm No. ISO 9613-1). (1993, 06).

Aures, W. (1985). Procedure for calculating the sensory euphony of arbitrary sound signal. In German: Berechnungsverfahren für den sensorischen Wohlklang beliebiger Schallsignale. *Acustica*, *59*(2), 130–141. Retrieved from https://www.ingentaconnect.com/contentone/dav/aaua/1985/00000059/00000002/art00008

Bernschütz, B. (2013, 03). A spherical far field HRIR/HRTF compilation of the neumann KU 100. *Proceedings of the 39th DAGA*, 592-595.

Chen, F., Gu, Z., Xie, H., & Wang, Z. (2006). Effects of compound-lean stator clocking in a low-speed axial compressor. *Journal of Propulsion and Power*, *22*(6), 1424-1426. Retrieved from https://arc.aiaa.org/doi/abs/10.2514/1.17591 doi: 10.2514/1.17591

Daniel, P., & Webber, R. (1997). Psychoacoustical Roughness: Implementation of an Optimized Model. *Accustica – acta acustica*, *83*, 113–123.

De Vries, R., van Arnhem, N., Sinnige, T., Vos, R., & Veldhuis, L. L. (2021). Aerodynamic interaction between propellers of a distributed-propulsion system in forward flight. *Aerospace Science and Technology*, *118*, 107009. doi: 10.1016/j.ast.2021.107009

Di, G.-Q., Chen, X.-W., Song, K., Zhou, B., & Pei, C.-M. (2016). Improvement of Zwicker's psychoacoustic annoyance model aiming at tonal noises. *Applied Acoustics*, *105*, 164–170. doi: 10.1016/j.apacoust.2015.12.006

d. Monteiro, F., Merino-Martinez, R., & Pereira, L. T. L. (2024). Psychoacoustic evaluation of an array of distributed propellers under synchrophasing operation. *30th AIAA/CEAS Aeroacoustics Conference (2024)*. Retrieved from https://arc.aiaa.org/doi/abs/10.2514/6.2024-3321 doi: 10.2514/6.2024-3321

Duivenvoorden, R. R., Sinnige, T., & Veldhuis, L. L. (2025). Impact of helix characteristics on slipstream deformation in propeller–wing–flap interaction. *AIAA Journal*, *63*(11), 4798–4817. doi: 10.2514/1.J064763

EASA. (2023). Environmental protection technical specifications applicable to VTOL-capable aircraft powered by tilting rotors. *consultation paper*, *1*. Retrieved from https://www.easa.europa.eu/en/document-library/product-certification-consultations/consultation-paper-environmental-protection-0

Ecma International. (2025). *ECMA-418-2:2025 Psychoacoustic metrics for ITT equipment — Part 2 (methods for describing human perception based on the Sottek Hearing Model)* (International standard No. 4th ed.) Ecma International. Retrieved from https://ecma-international.org/publications-and-standards/standards/ecma-418

Fastl, H., & Zwicker, E. (2007). *Psychoacoustics – Facts and models* (Third ed.). Springer Series in Information Sciences. Retrieved from https://www.springer.com/gp/book/9783540231592 (ISBN: 987–3–540–68888–4)

Greco, G. F., Merino-Martinez, R., Osses, A., & Langer, S. C. (2023). SQAT: a MATLAB-based toolbox for quantitative sound quality analysis. In 52^{th} *international congress and exposition on noise control engineering, august 20 – 23 2023, chiba, greater tokyo, japan.* International Institute of Noise Control Engineering (I-INCE). Retrieved from https://www.researchgate.net/publication/373334884_SQAT_a_MATLAB-based_toolbox_for_quantitative_sound_quality_analysis

Greco, G. F. and Merino-Martinez, R. and Osses, A. and Lotinga, M.J.B. (2025, Apr). *SQAT: a sound quality analysis toolbox for MATLAB (version v1.3).* Retrieved from https://zenodo.org/records/15148618 (Accessed in April 2025) doi: 10.5281/zenodo.7934709

Guérin, S., & Tormen, D. (2023). A contribution to the investigation of acoustic interferences in aircraft distributed propulsion. *CEAS Aeronaut J*, *14*, 965–982. Retrieved from https://link.springer.com/article/10.1007/s13272-023-00679-6 doi: 10.1007/s13272-023-00679-6

ISO norm 532–1 – Acoustics – Method for calculating loudness – Zwicker method (Tech.

Rep. No. 1). (2017). International Organization for Standardization. Retrieved from https://www.iso.org/obp/ui/#iso:std:iso:532:-1:ed-1:v2:en
Joseph, P., Morfey, C. L., & Lowis, C. R. (2003). Multi-mode sound transmission in ducts with flow. *Journal of Sound and Vibration*, *264*(3), 523–544. doi: 10.1016/S0022-460X(02)01205-1
Kamiyoshi, S., & Kaji, S. (2000). Tone noise reduction of multi-stage fan by airfoil clocking. *6th Aeroacoustics Conference and Exhibit*. Retrieved from https://arc.aiaa.org/doi/abs/10.2514/6.2000-1992 doi: 10.2514/6.2000-1992
Lafuente, A. P., Pulzovan, A. L., Cepeda-Gomez, R., & Geyer, T. F. (2025). Dynamic propeller noise reduction using synchrophasing control based on an extremum-seeking algorithm. *AIAA AVIATION FORUM AND ASCEND 2025*. Retrieved from https://arc.aiaa.org/doi/abs/10.2514/6.2025-3645 doi: 10.2514/6.2025-3645
Merino-Martinez, R., & Buzetelu, V. (2025). Aircraft noise-induced annoyance analysis using psychoacoustic listening experiments. In 11^{th} *forum acusticum euronoise conference, june 23 – 26 2025, málaga, spain.* doi: 10.61782/fa.2025.0112
Merino-Martinez, R., Pieren, R., & Schäffer, B. (2021, May). Holistic approach to wind turbine noise: From blade trailing–edge modifications to annoyance estimation. *Renewable and Sustainable Energy Reviews*, *148*(111285), 1–14. Retrieved from https://doi.org/10.1016/j.rser.2021.111285 doi: 10.1016/j.rser.2021.111285
Merino-Martinez, R., Yupa-Villanueva, R. M., von den Hoff, B., & Pockelé, J. S. (2024). Human response to the flyover noise of different drones recorded in field measurements. In 3^{rd} *quiet drones conference, september 8 – 11 2024, manchester, united kingdom.*
Milidonis, K., Semlitsch, B., & Hynes, T. (2018). Effect of clocking on compressor noise generation. *AIAA Journal*, *56*(11), 4225-4231. Retrieved from https://doi.org/10.2514/1.J057256 doi: 10.2514/1.J057256
More, S., & Davies, P. (2010). Human responses to the tonalness of aircraft noise. *Noise Control Engineering Journal*, *58*(4), 420-440. doi: 10.3397/1.3475528
Moreau, A., Prescher, A., Schade, S., Dang, M., Jaron, R., & Guérin, S. (2023). A framework to simulate and to auralize the sound emitted by aircraft engines. *InterNoise conference 2023*, *conference proceedings*.
Osses, A., García León, R., & Kohlrausch, A. (2016). Modelling the sensation of fluctuation strength. In 22^{nd} *international congress on acoustics (ica), september 5 – 9 2016, buenos aires, argentina.* Retrieved from https://pure.tue.nl/ws/portalfiles/portal/52366479/Osses_Garcia_Kohlrausch_ICA2016_ID113.pdf
Osses, A., Greco, G. F., & Merino-Martinez, R. (2023). Considerations for the perceptual evaluation of steady-state and time-varying sounds using psychoacoustic metrics. In 10^{th} *Convention of the European Acoustics Association (Forum Acusticum), September 11 – 15 2023, Torino, Italy.* doi: 10.61782/fa.2023.0600
Pascioni, K. A., Rizzi, S. A., & Schiller, N. (2019). Noise reduction potential of phase control for distributed propulsion vehicles. *AIAA Scitech 2019 Forum*. Retrieved from https://arc.aiaa.org/doi/abs/10.2514/6.2019-1069 doi: 10.2514/6.2019-1069
Patterson, A., Ackerman, K. A., Hovakimyan, N., & Gregory, I. M. (2021). Trajectory generation for distributed electric propulsion vehicles with propeller synchronization. *AIAA Scitech 2021 Forum*. Retrieved from https://arc.aiaa.org/doi/abs/10.2514/6.2021-0586 doi: 10.2514/6.2021-0586
Prescher, A., Moreau, A., & Schade, S. (2024). Model extension of random atmospheric inhomogeneities during sound propagation for engine noise auralization. *CEAS Aeronautical Journal*, *15*, 1111-1125. doi: 10.1007/s13272-024-00764-4
Schade, S., Jaron, R., Klähn, L., & Moreau, A. (2024). Smart blade count selection to align modal propagation angle with stator stagger angle for low-noise ducted fan designs. *Aerospace*, *11*(4), 259. doi: 10.3390/aerospace11040259
Schade, S., Ludowicy, J., Ratei, P., Hepperle, M., Stürmer, A., Schulze, P., . . . Geyer, T. F. (2026). Conceptual design of electrically powered urban air mobility vehicles for psychoacoustic studies. *Aerospace*, *13*(4). Retrieved from https://www.mdpi.com/2226-4310/13/4/312 doi: 10.3390/aerospace13040312
Tapken, U., Caldas, L., Meyer, R., Behn, M., Klähn, L., Jaron, R., & Rudolphi, A. (2021). Fan test rig for detailed investigation of noise generation mechanisms due to inflow disturbances. *AIAA AVIATION 2021 FORUM*. doi: 10.2514/6.2021-2314
Tapken, U., Gutsche, D., & Enghardt, L. (2014). Radial mode analysis of broadband noise

in flow ducts using a combined axial and azimuthal sensor array. *20th AIAA/CEAS Aeroacoustics Conference*. doi: 10.2514/6.2014-3318

Virtanen, P., Gommers, R., & Oliphant, T. (2020). Scipy 1.0: fundamental algorithms for scientific computing in python. *Nat Methods*, *17*, 261–272. doi: 10.1038/s41592-019-0686-2

von Bismark, G. (1974). Sharpness as an attribute of the timbre of steady sounds. *Acta Acustica united with Acustica*, *30*(3), 159–172. Retrieved from https://www.semanticscholar.org/paper/Sharpness-as-an-attribute-of-the-timbre-of-steady-Bismarck/9576a2a74bff46ee0cded25bfd9e4302b4fb0470

Zarri, A., Koutsoukos, A., & Avallone, F. (2023). Aerodynamic and acoustic interaction effects of adjacent propellers in forward flight. *AIAA AVIATION 2023 Forum*. Retrieved from https://arc.aiaa.org/doi/abs/10.2514/6.2023-4489 doi: 10.2514/6.2023-4489